

CB17: Inferring the dynamical history of a prestellar core with chemo-dynamical models

Ya. Pavlyuchenkov

Max Planck Institute for Astronomy, Königstuhl 17, D-69117 Heidelberg, Germany

pavyar@mpia.de

D. Wiebe

Institute of Astronomy of the Russian Academy of Sciences, 48, Pyatnitskaya Str., Moscow, 119017, Russia

dwiebe@inasan.ru

R. Launhardt

Max Planck Institute for Astronomy, Königstuhl 17, D-69117 Heidelberg, Germany

rлаu@mpia.de

and

Th. Henning

Max Planck Institute for Astronomy, Königstuhl 17, D-69117 Heidelberg, Germany

henning@mpia.de

ABSTRACT

We present a detailed theoretical study of the isolated Bok globule CB17 (L1389) based on spectral maps of CS, HCO⁺, C¹⁸O, C³⁴S, and H¹³CO⁺ lines. A phenomenological model of prestellar core evolution, a time-dependent chemical model, and a radiative transfer simulation for molecular lines are combined to reconstruct the chemical and kinematical structure of this core. In addition we investigate the influence of various physical factors on molecular line profiles. It is shown that the intensity of the external UV field, the probability for molecules to stick onto dust grains, the core age, and the rotation velocity all significantly affect the molecular line spectra. Due to this influence, the asymmetry of optically thick lines allows to remove the ambiguity between the sticking probability

and the core age. We demonstrate that these parameters are well constrained, when results of the modeling are compared to observations in multiple lines of sight through the core. We developed a general criterion that allows to quantify the difference between observed and simulated spectral maps. By minimizing this difference, we find that very high and very low values of the effective sticking probability S are not appropriate for the studied prestellar core. The most probable S value for CB17 is 0.3–0.5. The spatial distribution of the intensities and self-absorption features of optically thick lines is indicative of UV irradiation of the core. By fitting simultaneously optically thin transitions of C^{18}O , H^{13}CO^+ , and C^{34}S as well as optically thick transitions of HCO^+ and CS , we isolate the model that reproduces all the available spectral maps to a reasonable accuracy and, thus, represents a good approximation to the core chemical and kinematical structure. The line asymmetry pattern in CB17 is reproduced by a combination of infall, rotation, and turbulent motions with velocities $\sim 0.05 \text{ km s}^{-1}$, $\sim 0.1 \text{ km s}^{-1}$, and $\sim 0.1 \text{ km s}^{-1}$, respectively. These parameters corresponds to energy ratios $E_{\text{rot}}/E_{\text{grav}} \approx 0.03$, $E_{\text{therm}}/E_{\text{grav}} \approx 0.8$, and $E_{\text{turb}}/E_{\text{grav}} \approx 0.05$ (the rotation parameters are determined for $i = 90^\circ$). The chemical age of the core is about 2 Myrs. In particular, this is indicated by the central depletion of CO , CS , and HCO^+ . On the other hand, the depletion is not strong enough to show up in intensity maps as a ring-like pattern. Based on the angular momentum value, we argue that the core is going to fragment, i.e., to form a binary (multiple) star.

Subject headings: astrochemistry — line: profiles — stars: formation — ISM: molecules — ISM: individual (CB17)

1. Introduction

Of all the diverse steps of the star formation process, the prestellar stage is supposed to be the most quiescent phase. Starless cores are nearly isothermal, have more or less regular shapes, and lack prominent kinematic features, like disks and outflows. Among those cores, Bok globules are especially attractive for studies, as they are relatively isolated from a confusing surrounding material and, thus, represent ‘clean’ examples of the prestellar chemical and dynamical evolution. Numerous embedded and isolated starless cores have been subjects of chemical and kinematical studies during recent years. As we generally want to know if these cores are going to become stars eventually or, in other words, if they are not only starless but really prestellar, these studies are mainly directed toward the search for infall signatures. A commonly used collapse indicator is the characteristic blue-red line

asymmetry of optically thick lines (Evans 1999). Usually, the central spectrum of a core is utilized to demonstrate that this asymmetry is present.

However, if one wants to investigate the kinematics in more detail, it is necessary to observe and to analyze spectra at locations offset from the center of a core. 1D spectral cuts or 2D spectral maps are employed in various ways. Spectral maps for several molecules have allowed Tafalla et al. (1998) to detect an extended infall in the now famous L1544 prestellar core. This study has later been followed by Williams et al. (1999), who have used N_2H^+ spectral maps to investigate the infall in the very center of the core. Mapping surveys for infall motions in a number of starless cores have been carried out by Gregersen & Evans (2000) in lines of HCO^+ and by Lee et al. (2001) in lines of CS, CO, and N_2H^+ .

Another goal of investigating spectral maps is the study of rotation of starless cores, where both red and blue asymmetric line profiles are present. E.g., Kane & Clemens (1997) have studied the rotation in fifteen starless Bok globules based on CO maps, while Pavlyuchenkov & Shustov (2004) have used HCO^+ spectral maps, obtained by Gregersen & Evans (2000), to determine the average rotation speed (as well as the shape and the infall speed) for the L1544 core. Pavlyuchenkov & Shustov (2004) assumed that the core collapses from the initial rigid rotation state so that its total angular momentum remains constant. The spatial separation of red and blue asymmetric HCO^+ line profiles in the maps of the L1689B prestellar core has been reproduced with a 3D molecular line radiation transfer model by Redman et al. (2004). They showed that the asymmetry in this core can be explained under the assumption of solid-body rotation in the core center. At a later evolutionary stage, the rotation and infall profiles for the very young protostar IRAM 04191 have been determined by Belloche et al. (2002) from CS spectral maps.

A more comprehensive analysis of spectral maps is also possible. Lada et al. (2003) interpreted the alternating asymmetry pattern in CS spectral lines observed in B68 as a signature of simultaneous inward and outward motions having both radial and non-radial modes. Tafalla et al. (2004) performed a similar study of the L1498 and 1517B prestellar cores. Using N_2H^+ and NH_3 spectral maps they investigated velocity gradients across the core faces and found them indicative of a velocity pattern more complicated than just infall or rotation. They suggested that this pattern is associated with asymmetric gas motions resulting from residual core collapse. These results indicate clearly that, given the overall quest for infall in starless cores, a great care must be taken to avoid confusion between infall and other bulk motions. They also stress that detailed kinematic information on starless cores is necessary to draw any conclusion about their dynamical and evolutionary state.

The spectral maps are not the only ingredient needed for an analysis of the starless core kinematics. To serve this purpose they have to be complemented by some knowledge on

the core chemical composition. The uniform abundances of tracer molecules over the core are now confidently rejected both on observational (e.g., Tafalla et al. 2002) and theoretical (Rawlings & Yates 2001) grounds. It is now customary to reproduce observations with some simplified representation of a radial abundance profile (like a step function, for example). However, Lee et al. (2005) showed that simple empirical distributions may not be good indicators of the real chemical structure in collapsing cores. But if they would be, these simple distributions do not contain information about the dynamical and chemical history of the core. Rawlings & Yates (2001) argued that only multiple line-of-sight observations coupled to detailed chemical models are able to shed light on prestellar evolution.

This is the approach we adopt here, utilizing detailed spectral maps in a number of transitions for the CB17 core. This core is located at the south-east edge of a small isolated, and slightly elongated globule at a distance of about 300 pc. Several authors have studied its chemical composition, but the most extensive investigation has been performed by Turner and co-authors (Turner 1995, 1996; Turner et al. 1997, 1998). They argued that the chemical composition of this core is in many respects unusual, with overabundant HCO^+ , N_2H^+ , HC_3N , and some other species. However, it must be noted that their study has been focused on small translucent clouds. When compared to other dense cores, the CB17 core shows typical column densities of N_2H^+ (Benson et al. 1998; Caselli et al. 2002) and ammonia (Lemme et al. 1996).

Using molecular line maps, we study in this paper abundances of CO, HCO^+ , and CS as a function of distance from the core center. We choose a detailed chemical model to compute the time-dependent abundances at a number of locations within the core, assuming its spherical symmetry. Both static and dynamically evolving configurations are considered. These abundances are then used to simulate the spectral maps that are directly compared to the observed line profiles.

The attempt to reproduce the observed state of the core as an outcome of the time- and depth-dependent chemical model is hampered by the presence of many unknown or poorly known parameters. At first sight, it may seem they can be adjusted almost arbitrarily to get the best agreement with observations. However, this is not exactly the case when multiple lines of sight are analyzed. The most important parameters for the chemical model are the probability S for species to stick to dust grains and the intensity G of the UV field that illuminates the core, as they control abundances in the inner and outer regions of a core, respectively. Two remarks should be made about these parameters. First, the sticking probability S represents an effective value which is valid as long as there are no desorption mechanisms other than those considered in the paper (thermal desorption, cosmic ray desorption, photodesorption). In the case that some powerful evaporation mechanism is

missing in the model, the best-fit S value would be higher than that quoted in the Abstract. Second, rates of photoreactions can be different from the rates used in the model if the spectral properties of the UV field in the core vicinity differ significantly from the average interstellar field.

We consider a range of these parameters and demonstrate that their values can be significantly constrained if a comparison with observations is not limited to just a central spectrum. Using a static model, we find the value of G that allows to reproduce the observations most reasonably. This value is then used as an input for the dynamical model. Instead of fixing a certain contraction law, we consider a range of *ad hoc* solutions to check if the dynamical history of a core leaves some observable imprint on its chemical structure and emergent line profiles. With the dynamical model we estimate the sticking probability, the age of the core, the infall velocity, and the rotation velocity. In particular, we show that the asymmetry of the line profiles can be used to relax the ambiguity between the sticking probability and the core age.

The structure of the paper is as follows. In § 2 we describe the chemical model and the formalism that is used to simulate the core dynamical evolution. The radiation transfer model, the criterion for the comparison with observations, and the used observational data are also presented in § 2. Results of the chemical modeling for the static core model are given in § 3. The dynamical models with and without rotation are presented in § 4. Our results are discussed in § 5 and summarized in § 6.

2. Model

In general, we expect that the dynamical evolution of a prestellar core is related to its chemical evolution via the time-dependent density, extinction etc. Thus, we want to address the question if simulations of the chemical evolution are a good tool to get insights into the dynamical history of the core. For that, we consider a model of a collapsing and rotating cloud, which provides us with the time-dependent density and velocity fields. This model is combined with an appropriate chemical model in order to find the representation of the core that provides the best agreement with the observed spectral maps. A straightforward way is to parameterize the problem and then to use some criterion that quantifies the difference between the observed and theoretical spectra. Given the large number of parameters, we split the problem in three parts.

In a first step, we investigate the ‘chemical’ parameters with a static configuration in which the core has zero regular velocity, and the density distribution stays constant with time

and is equal to the observed current state (see § 2.1.1). Ignoring the dynamical evolution, this model represents a convenient way to study purely ‘chemical’ factors which must be taken into account, when analyzing molecular line spectra. Specifically, the static model is used to constrain the intensity G of the UV field in the vicinity of the core.

In a second step, the best-fit G value is used in a 1D collapse model, in which a phenomenological way is adopted to describe a time-dependent density structure. This technique is by no means hydrodynamical in nature. However, it allows to probe a wider range of collapse regimes than more physical approaches taken by, e.g., Shematovich et al. (2003) or Aikawa et al. (2005). At this step we consider only the central spectrum as it is not affected by rotation. This analysis permits the selection of a collapse mode that is the best in reproducing the central line asymmetry.

In a third step, the best-fit dynamical model is used as an input for the model with both collapse and rotation. With this model we determine the rotation velocity and the position angle. A flow chart of these steps is presented in Figure 1.

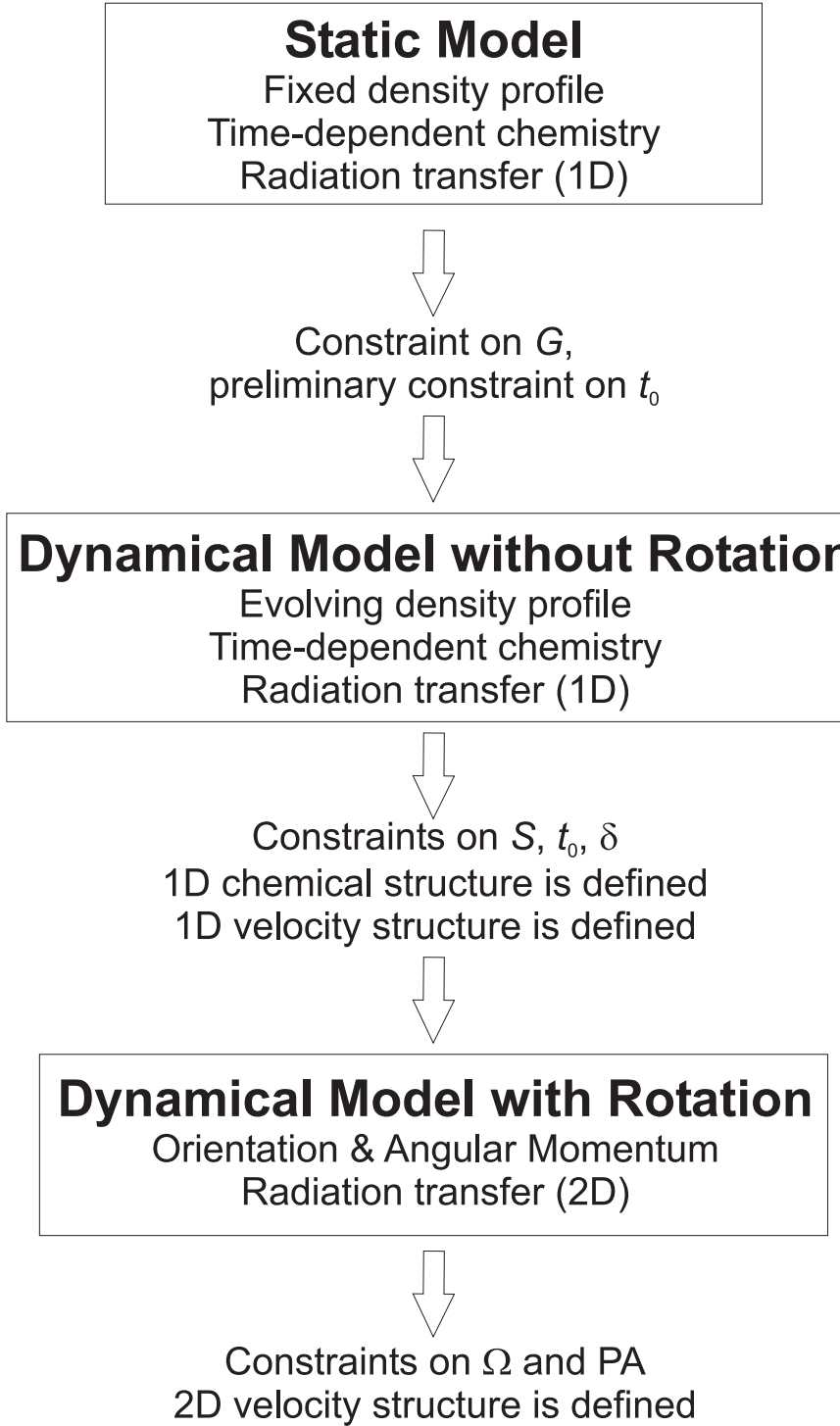


Fig. 1.— The flowchart of the technique used in the paper.

In the following, we describe both the static and non-static models in detail, together with the adopted models of the chemical evolution and the line radiation transfer. A criterion is presented that is used to compare modeled and observed spectral line maps. For this comparison, we consider the optically thin transitions $\text{C}^{34}\text{S}(2-1)$, $\text{H}^{13}\text{CO}^+(1-0)$, and $\text{C}^{18}\text{O}(2-1)$ as well as the optically thick transitions $\text{CS}(2-1)$, $\text{HCO}^+(1-0)$, for which most complete spectral maps are available. As we have one transition per isotopomer, hereafter we omit the transition designation.

Observations of various molecular emission lines towards CB 17 for isotopes and transitions of CO, CS, and HCO^+ were performed in June 1993 and October 1996 using the IRAM 30-m telescope. Final calibration and data reduction were done with the CLASS software, which is part of the GILDAS¹ package. Since different nominal center positions as well as v_{LSR} were used in different years, and some of the maps were done with a smaller spatial sampling for the central part of the dense core than for the outer regions, all spectra of a given line were combined and resampled on a regular spatial and frequency grid using a gaussian beam of HPBW and channel width listed in Table 1. The reference position (0,0) for all data and maps in this paper is RA = 04:00:32.90, DEC = 56:47:52.0 (B1950). These observations represent part of an extensive study of the CB17 core in many molecules and transitions which will be described in full detail in another paper (Launhardt et al., in preparation).

¹The GILDAS working group is a collaborative project of Observatoire de Grenoble and IRAM, and comprises: G. Buisson, L. Desbats, G. Duvert, T. Forveille, R. Gras, S. Guilloteau, R. Lucas, and P. Valiron.

Table 1: Spectral line parameters at peak position (-1'',+8'')

Line	HPBW, arcsec	$\Delta v_{\text{chann}}, \text{m s}^{-1}$	$v_{\text{LSR}}, \text{km s}^{-1}$
C ¹⁸ O (2–1)	11	100	-4.73
CS (2–1)	25	70	-4.68
C ³⁴ S (2–1)	25	65	-4.59
HCO ⁺ (1–0)	27	65	-4.67
H ¹³ CO ⁺ (1–0)	29	65	-4.64

To compare models and observations we need to define velocity shift for modeled spectra, i.e. V_{LSR} , which represents velocity of a model core with respect to an observer. Obviously, this value should be the same for all the studied lines. However, gaussian fit to the observed profiles toward the center of the core produces different V_{LSR} values for various lines (between -4.59 and -4.73 km s $^{-1}$, Table 1). Within the framework of our approach we cannot explain this scatter of V_{LSR} for central profiles. On the other hand, differences in observed V_{LSR} values may be caused not by a presumably complex structure of the core but rather by somewhat incorrect values of rest frequencies for the studied transitions.

For simplicity, in our calculations we adopt $V_{\text{LSR}} = -4.7$ km s $^{-1}$ for $\text{HCO}^+(1-0)$, $\text{CS}(2-1)$, and C^{18}O , and $V_{\text{LSR}} = -4.6$ km s $^{-1}$ for $\text{H}^{13}\text{CO}^+(1-0)$, $\text{C}^{34}\text{S}(2-1)$.

2.1. Morphology and Dynamics

2.1.1. Static Core

The density structure of a prestellar core can generally be approximated by (e.g., Tafalla et al. 2002)

$$n(\text{H}_2) = \frac{n_0}{1 + (r/r_0)^\beta}, \quad (1)$$

where n_0 is the central density, r_0 is the radius, where n has dropped to half the central density (i.e., the size of an inner density plateau), and β is the power law index which describes the density fall-off in the outer parts of the core. We use equation (1) to describe the observed density profile of the CB17 core with parameters $n_0 = 5.4 \cdot 10^5$ cm $^{-3}$, $r_0 = 3000$ AU, and $\beta = 2.2$ as derived in Launhardt et al. (in preparation). In addition, we use an outer cut-off radius which is taken to be $2.5 \cdot 10^4$ AU, the estimated radius of the CB17 core. The gas temperature in the CB17 core is assumed to be uniform and equal to $T = 10$ K.

In the static model the core evolves only chemically, with an evolutionary time t_0 . In physical terms, this model corresponds to the situation where the core forms almost instantly (with the formation timescale significantly shorter than the chemical timescale) and then stays static for its entire lifetime. In the absence of a systematic velocity, the width of line profiles is determined by microturbulent velocity V_{turb} , which is taken to be 0.15 km s $^{-1}$ over the entire core in order to reproduce the observed line width.

2.1.2. *Collapsing Core*

The static model does not provide a complete description of a typical starless core, as many such cores (including CB17) show clear signs of internal dynamics. Molecular abundances certainly do not only depend on the core density and ‘chemical’ age, but rather represent the result of its entire previous chemo-dynamical evolution. This is why almost all recent chemical studies of prestellar cores are coupled in some way or another to dynamical models (e.g., Shematovich et al. 2003; Aikawa et al. 2005; Lee et al. 2005; Flower et al. 2005). In this paper we do not stick to any particular dynamical solution. Instead we choose a phenomenological approach that allows to describe the core evolution with only a few parameters.

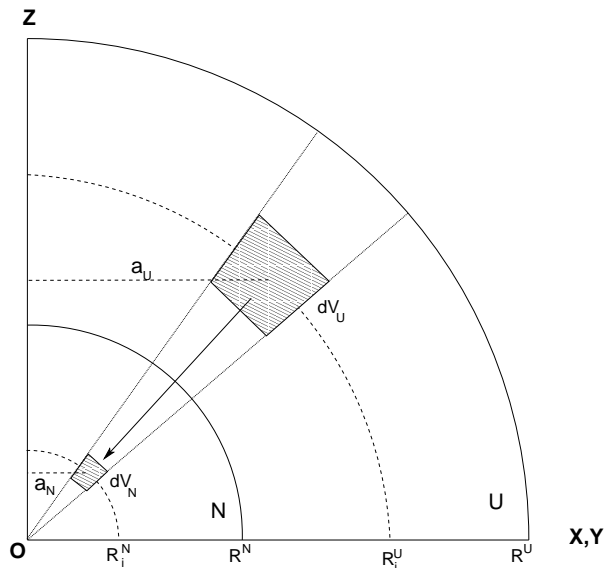


Fig. 2.— Phenomenological model of the starless core evolution. R^U is the radius of the initially uniform core, R^N is the radius of the non-uniform (observed) core. The volume element dV_U during collapse evolves to the volume element dV_N .

As in the static model, we assume that the non-uniform ('N') density distribution (1) represents the current, observed state of the core. In this configuration, the model core is divided into 48 concentric shells of equal width, having radii R_i^N . In the initial uniform ('U') state the model core is spherically symmetric and has the constant initial density $n_U = 5 \cdot 10^3 \text{ cm}^{-3}$ (Figure 2), which is close to the typical gas density in the vicinity of the core. Our results are not sensitive to small variations of this parameter. Locations of shell boundaries in the 'U'-configuration are determined by the requirement that each shell has the same mass as in the final state, i.e. the initial radius of each shell R_i^U is uniquely defined by the assumed n_U . The time scale for the evolution of the system, needed for configuration 'U' to evolve to configuration 'N', is t_0 . At any moment t the location of the i th shell is defined by

$$R_i(t) = R_i^U - W_i \left(\frac{t}{t_0} \right)^\delta \quad (2)$$

where W_i is defined by the condition $R_i(t_0) = R_i^N$, so that $W_i = R_i^U - R_i^N$. Using equation (2), we compute the density of each shell as a function of time and use this in the chemical model. The radial velocity of shell i at time t_0 is

$$V_i(t_0) = -\delta \frac{W_i}{t_0}, \quad (3)$$

Thus, the velocity only depends on the δ/t_0 ratio, given the initial density is fixed. The power law index δ in equation (2) allows to describe different regimes of the core collapse without going into details of an underlying physical model.

As an example, in Figure 3 we show plots for the central density evolution and the radial velocity profiles in models with $t_0 = 10^6$ years and various values of δ . A nearly linear growth of the central density corresponds to $\delta = 0.1$. At smaller δ , density accumulation decelerates with time; at $\delta > 0.1$ the density first stays almost constant, but then grows faster and faster. The static model corresponds to $\delta = 0$.

This model is similar in concept to other generalized prescriptions given, e.g., by Whitworth & Ward-Thompson (2001) or Myers (2005). It is also close (for $\delta \approx 2$) to the destabilized Bonnor-Ebert sphere collapse model used by Aikawa et al. (2005), which is also shown in Figure 3. The velocity profile in our model is shallower and shows less tendency to peak at the near-core region. This is caused by a different choice of initial conditions, specifically, by the uniform initial density distribution.

This prescription for the core contraction may not satisfy the momentum equation strictly and is therefore potentially inconsistent. However, our intention here is more to demonstrate, that it is possible in principle to distinguish different regimes of the core evolution using observations of molecular lines, rather than to give support to some self-consistent

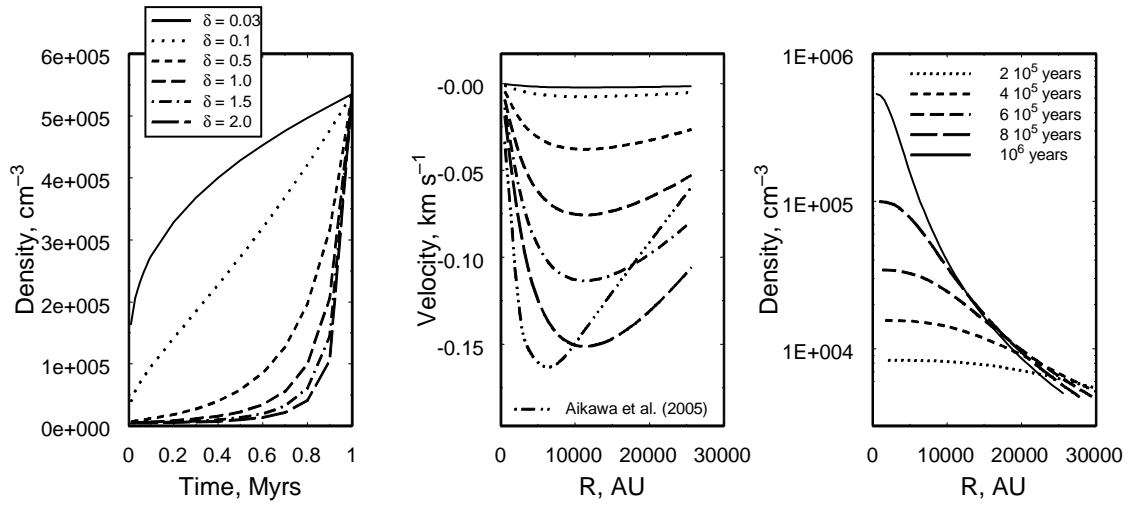


Fig. 3.— Dynamical structure of the model core. (left) Time evolution of the central number density for $t_0 = 10^6$ years and different values of δ . (middle) Radial velocity profiles for different values of δ at the end of evolution ($t_0 = 10^6$ years) compared to the velocity profile from Aikawa et al. (2005) for their $\alpha = 1.1$ and $t = 1.15 \times 10^6$ years. Same legend applies as in left panel. (right) The density profile evolution for $t_0 = 10^6$ years and $\delta = 1$. The density distribution at the last time moment corresponds to that inferred for the CB17 core.

solution. Also, the dynamics of prestellar cores can be influenced by magnetic fields and/or turbulence, so that the simplest form of momentum equation for spherical isothermal collapse may not be satisfied anyway. Using this approach, it may be possible to find the extent to which the momentum conservation in collapsing cores is affected by non-thermal supporting factors.

2.1.3. Collapsing Core with Rotation

Even though the rotation of starless cores does not influence their (early) dynamical evolution it affects molecular line profiles. The CB17 core is likely to have a significant angular momentum, which shows up as an alternating asymmetry pattern across the core face.

We include rotation into the phenomenological model, assuming that a toroidal element dV_U of a shell (Figure 2), initially located at a distance a_U from the rotation axis, moves during collapse so that its angular momentum is conserved, i.e. that the momentum is not redistributed over the core. This is a good approximation as long as there is no magnetic braking or turbulent momentum transport. We assume that the core initially rotates as a solid body with the angular velocity Ω , so the azimuthal velocity at t_0 is

$$V_\phi = \frac{\Omega a_U^2}{a_N}, \quad (4)$$

where a_U and a_N are radii of a toroidal element in configurations ‘U’ and ‘N’. Each of the 48 shells is subdivided into 32 angular cells. This model is used in the following to estimate the angular momentum of the CB17 core and to derive its spatial orientation.

2.2. Chemical Model

The model for the chemical evolution of the core is described by Wiebe et al. (2003) and Semenov et al. (2004). We refer the reader to these papers for more details. Here only the main features of the model are summarized. The model is a time-dependent chemical model which includes gas-phase reactions as well as the freezing-out of molecules onto dust grains and their desorption back to the gas-phase. For simplicity, all grains are assumed to have the same radius of 10^{-5} cm. Surface reactions are not taken into account in the current study.

Gas-phase reactions are taken from the UMIST95 ratefile (Millar et al. 1997). We consider the evolution of species containing H, He, C, N, O, Mg, Na, Fe, S, and Si atoms.

For the cosmic rate ionization rate the standard value of $1.3 \times 10^{-17} \text{ s}^{-1}$ is assumed. The UV-flux for photo-reaction rates is expressed by the G factor measured in units of the average interstellar flux (Draine 1978). We are aware that the spectrum of the radiation field in star-forming regions may differ quite significantly from the average interstellar spectrum. The relative ‘hardness’ of a spectrum affects the photoreaction rates. However, the study of this effect is beyond the scope of the present paper. The CB17 core is quite isolated, so that there are no young massive stars nearby and no obscuring molecular cloud is present. Thus, the spectrum of the radiation field should be similar to that of the interstellar field.

As in our dynamical model the density profile evolves, the extinction is evaluated as a function of time at each point of the flow as

$$A_V(r, t) = N_H(r, t) / 1.59 \times 10^{21} \text{ cm}^{-2},$$

where

$$N_H(r, t) = \int_r^R n(H) \text{d}r$$

is the column density of hydrogen nuclei measured from the core boundary R to a point at the radius r . H_2 self- and mutual shielding of CO and H_2 are taken into account using the results obtained by Lee et al. (1996). No attempt is made to account for the thermal balance in the medium. The model core is assumed to be isothermal at 10 K. This assumption breaks down at the core edge where the gas is heated by UV radiation. However this moderate heating would not affect the chemical reaction rates significantly. The same is true for the desorption from grains, as this region is dominated by photo-desorption.

Neutral species other than H_2 and He are assumed to stick to dust grains with the same probability S which is one of the parameters of our study. In addition to photo-desorption, thermal desorption and cosmic ray induced desorption are taken into account. Desorption energies are taken from Hasegawa & Herbst (1993).

At $t = 0$ all elements are present in atomic form with the only exception of hydrogen which is entirely bound in H_2 molecules initially. The ‘low metal’ initial abundance set from Wiebe et al. (2003) is used. The entire core is chemically uniform initially. After the onset of collapse, in the adopted Lagrangian description each gas parcel moves and evolves independently with the density varying according to the adopted dynamical prescription.

In our study we vary two parameters for the chemical model, namely, the strength of the external UV field G and the sticking probability S , which regulate the abundances of species in the outer envelope and in the core center, respectively.

As a test of the model, we compare it to results obtained by Aikawa et al. (2005).

The closest match to their model with $\alpha = 1.1$ (see Aikawa et al. 2005, for details) and central density of $3 \times 10^6 \text{ cm}^{-3}$ is given by our dynamical model with $\delta \approx 2$ (Figure 3). For this comparison, we set $G = 1$, $S = 1$, $A_V = 3 \text{ mag}$ at the core edge and included surface reactions. Also, the branching ratio for the N_2H^+ dissociative recombination from Geppert et al. (2004) is taken into account. In Table 2 we compare column densities from this calculations to those given in Table 2 by Aikawa et al. (2005). We present both straight column densities toward the core center and the column densities convolved with a $40''$ Gaussian beam (HPBW; the distance of 300 pc is assumed). Given the variety of assumptions and the different underlying reaction sets (UMIST 95 and the NSM), the agreement seems to be reasonable.

Table 2: Molecular column densities for a representative dynamical model

Species	Aikawa et al. (2005)	This work	This work, with convolution
CO	1.9(17)	6.3(16)	7.1(16)
HCO ⁺	2.9(13)	1.2(13)	1.3(13)
HCN	8.0(14)	3.6(14)	2.3(14)
HC ₃ N	5.8(12)	4.7(13)	3.9(13)
NH ₃	7.8(15)	4.1(15)	1.5(15)
N ₂ H ⁺	1.8(13)	8.4(13)	2.8(13)
CS	1.0(13)	4.5(13)	4.5(13)
C ₂ S	6.9(11)	2.2(12)	2.3(12)
C ₃ H ₂	8.7(12)	3.9(13)	3.6(13)

2.3. Radiative Transfer Model

The radiative transfer modeling is based on the solution of the radiative transfer (RT) equation coupled with balance equations for molecular level populations. We solve this system with the 1D/2D NLTE code ‘URAN(IA)’ developed by Pavlyuchenkov & Shustov (2004). This code partly utilizes the scheme originally proposed and implemented in the available 1D code ‘RATRAN’ (Hogerheijde & van der Tak 2000).

Here we only summarize the general concept of the ‘URAN(IA)’ code. The iterative algorithm is the following. First, initial molecular level populations and a set of photon random paths through the model space are defined. With these quantities, the specific intensities $I_\nu(i)$ are computed for each cell by the explicit integration of the RT-equation along the pre-defined photon paths $\vec{n}(i)$. Then, $\vec{n}(i)$ and $I_\nu(i)$ are used to calculate the mean line intensity \tilde{J} in each cell for all transitions. The computed mean intensities are utilized in the next iteration step to refine the level populations by solving balance equations in all model cells. To accelerate the convergence of the entire procedure for optically thick lines, additional internal subiterations for each grid cell (ALI scheme) are included on top of the global iterations. The adopted acceleration scheme uses the fact that the calculated mean line intensity at each particular cell can be divided into an internal component generated in the cell and the external contribution that comes from other cells of the grid. Subiterations are applied to bring into an agreement the internal mean intensity of the line and the corresponding level populations in each cell. After the final molecular level populations are obtained, we repeat the calculations, but with another set of pre-defined random photon paths in order to estimate a typical error in the computed values. In our simulations, relative errors in the level populations are not larger than 1%. Finally, the resulting level populations are used to calculate excitation temperatures, which are further transformed into synthetic beam-convolved single-dish spectra.

2.4. Evaluation of the Model Quality

The selection of criteria for a quantitative comparison of modeled and observed spectral maps represents an important step, but is a rather complicated problem. In a detailed analysis we would need to take into account a (dis)agreement of the various features and characteristics of the spectra, such as intensities, widths, asymmetries, shifts, dips, regularities in the spatial distributions, etc. These features can be either analyzed separately or incorporated into a common criterion with different weights. Using different features and criteria, based on them, we can assess different aspects of the consistency between the model and observations.

One of the commonly-used techniques to check the model is to compare distributions of observed and modeled integral line intensities over the core. This allows to judge how well a model reproduces the spatial distribution of the total energy that is emitted in a given transition, reflecting not only the total molecular content (and excitation conditions) but also the molecular distributions within the core.

Of course, minimization of this value does not guarantee the consistency between modeled and observed kinematic properties of the source because it does not account directly for widths, shifts, asymmetries which reflect the velocity field. To estimate if the model reproduces the kinematic structure, e.g., rotation of the core, one can compare the distributions of the mean velocities. In turn, such a comparison does not take into account the consistency of the line intensities.

In this paper the quality of the spectra fit is evaluated with the general criterion

$$SP = \frac{1}{J^{\text{obs}} + J^{\text{mod}}} \sum_{k=1}^{N_{\text{pos}}} \sum_{i=1}^{N_{\text{chan}}} |I_i^{k,\text{obs}} - I_i^{k,\text{mod}}| \Delta v_i. \quad (5)$$

The inner sum is the absolute difference between observed and modeled spectra at map position k , $I_i^{k,\text{obs}}$ and $I_i^{k,\text{mod}}$ are observed and theoretical intensities in velocity channel i , N_{chan} is the number of velocity channels, Δv_i is the channel width, and J^{obs} and J^{mod} are the observed and modeled intensities integrated over the frequency and over the map

$$J = \sum_{k=1}^{N_{\text{pos}}} \sum_{i=1}^{N_{\text{chan}}} I_i^k \Delta v_i. \quad (6)$$

SP is normalized so that $0 \leq SP \leq 1$.

To illustrate the behavior of this criterion, we consider the case of a single spectrum, when both observed and modeled line profiles are rectangular with equal width Δv and position v_0 , but with different intensities. In this case SP is equal to

$$SP = \frac{|J^{\text{obs}} - J^{\text{mod}}|}{J^{\text{obs}} + J^{\text{mod}}}. \quad (7)$$

The value of SP as a function of $J^{\text{obs}}/J^{\text{mod}}$ is shown in Figure 4. In the log-scale this function is symmetric relative to the point $J^{\text{obs}}/J^{\text{mod}} = 1$ where $SP = 0$. If intensities differ by a factor of 2 then $SP \approx 0.4$, while an order of magnitude difference gives $SP \approx 0.8$.

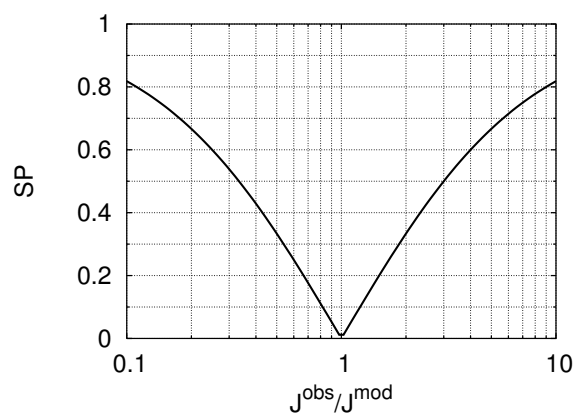


Fig. 4.— SP criterion as a function of $J^{\text{obs}}/J^{\text{mod}}$ for rectangular profiles.

SP, thus, describes the normalized deviation between modeled and observed line intensities averaged over all velocity channels and all map positions. On the other hand, SP no longer contains any information about the specific cause of a disagreement between the model and the observations.

3. Results for the static model

Here we consider three important parameters of the static model, namely, the total chemical evolution time t_0 , the sticking probability S , and the strength of the external UV field G . Regarding these quantities as free parameters we fit the observed spectra, considering the 3D parametric space of models with $0 < S < 1$, $0 < G < 1$, and $0.2 < t_0 < 2.0$ Myr, and calculated 330 models in total.

For each of these models, we calculate molecular abundances as a function of radius. Then, distributions of molecular abundances are used as input data for the RT model. As a result of the RT simulations, we obtain distributions of level populations over the core for molecules of interest, which are further transformed into spectral maps. All the synthetic line profiles in the map are convolved with Gaussian beams and shifted in accordance to the observed V_{LSR} position. Line profiles are calculated for those locations in the map where they have been observed. Finally, the SP criterion is checked for each model.

3.1. Overview of the Core Chemical Structure

Radial distributions of CO, CS, and HCO^+ abundances for the static model at $t = 0.2$ Myr and $t = 2.0$ Myr are shown in Figure 5. The overall chemical structure of the core is very similar to that obtained by Lee et al. (2005), cf. their Figure 9 (abundances for $t = 0$ in their model). The evolution of the CO abundance is quite simple. In the $S = 0$ case (just gas-phase chemistry) $x(\text{CO})$ is almost constant all over the core, being nearly equal to the total carbon abundance. The non-zero sticking probability leads to a noticeable CO freeze-out in the core and to a minor CO depletion in the envelope. In the case with UV illumination CO molecules in the envelope are almost totally dissociated.

The HCO^+ abundance is not very sensitive to the actual S value. The only parameter that can be more or less reliably constrained with observations of HCO^+ is G .

The CS abundance depends on all three parameters. The location of the dip in the radial CS profile, appearing in UV-illuminated models, coincides with the region of enhanced CO abundances, which decrease the number of carbon atoms available for CS formation.

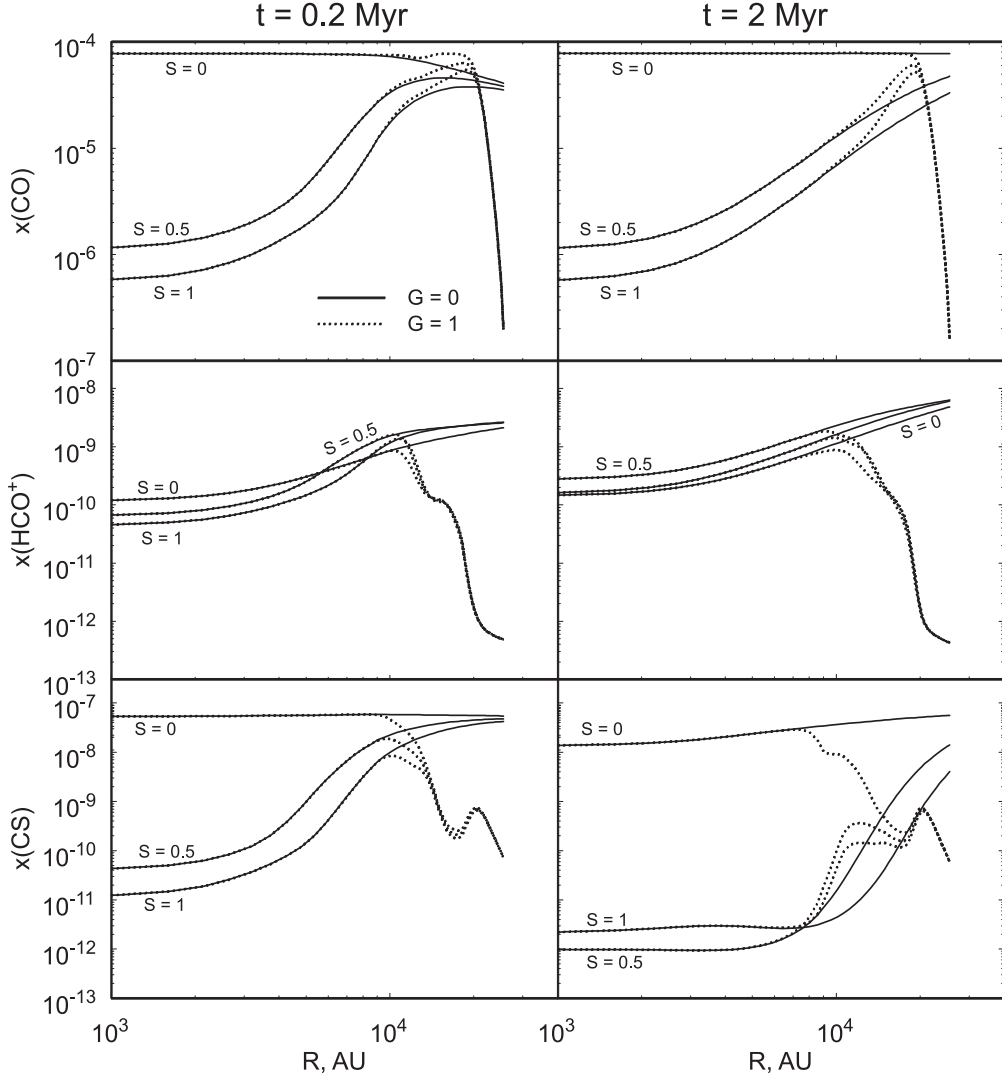


Fig. 5.— Radial distributions of CO (top panels), HCO^+ (middle panels), and CS (bottom panels) for the static model at a chemical evolution time $t = 0.2$ Myr (left column) and 2 Myr (right column). Shown are results for no UV and standard UV cases with sticking probabilities $S = 0, 0.5$, and 1 .

The discussed behaviour is not strongly time-dependent, being only slightly more pronounced at later times of the chemical evolution. We should note that the same general features are shared by dynamical models, which justifies our usage of line profiles in the static model as a guide for possible ranges of S and G .

3.1.1. Note on N-bearing Species

Before we analyze the CO, CS, and HCO^+ data, we discuss briefly our ability to match the other available observations, specifically, the data on N-bearing species that are not the main subject of the current study. The column density of N_2H^+ has been determined by Benson et al. (1998) and Caselli et al. (2002) to be $3 - 5 \times 10^{12} \text{ cm}^{-2}$. The column density of NH_3 is about $8 \times 10^{14} \text{ cm}^{-2}$ (Lemme et al. 1996; Jijina et al. 1999). Our values, compiled in Table 2, are somewhat higher for both molecules. Currently, our ability to treat these molecules with URAN(IA) is limited because of the poor knowledge of hyperfine transition parameters. We modeled the $\text{N}_2\text{H}^+(1-0)$ profile, neglecting its hyperfine structure and obtained antenna temperatures of the order of 0.4–0.6 K, similar to what is observed. We also performed an approximate modeling of the HCN (1–0) line and compared the result with the profile obtained by Turner et al. (1997). We are able to reproduce the antenna temperature and main features of the profile, in the sense that both the $F = 2 - 1$ and $F = 1 - 1$ transitions are self-absorbed, while the $F = 1 - 0$ transition is not self-absorbed. The intensity ratios in our model are different from those in Turner et al. (1997). Molecular data from Schöier et al. (2005) are used for this analysis.

3.2. Optically Thin Lines

We first analyze optically thin transitions that probe the total molecular content of the core. In order to show the fitting results in a compact way, we present them as ts -diagrams which are 2D-plots of SP-values for various t_0 and S parameters at a fixed G value. The ts -diagrams for optically thin transitions of C^{18}O , H^{13}CO^+ , and C^{34}S are shown in Figure 6.

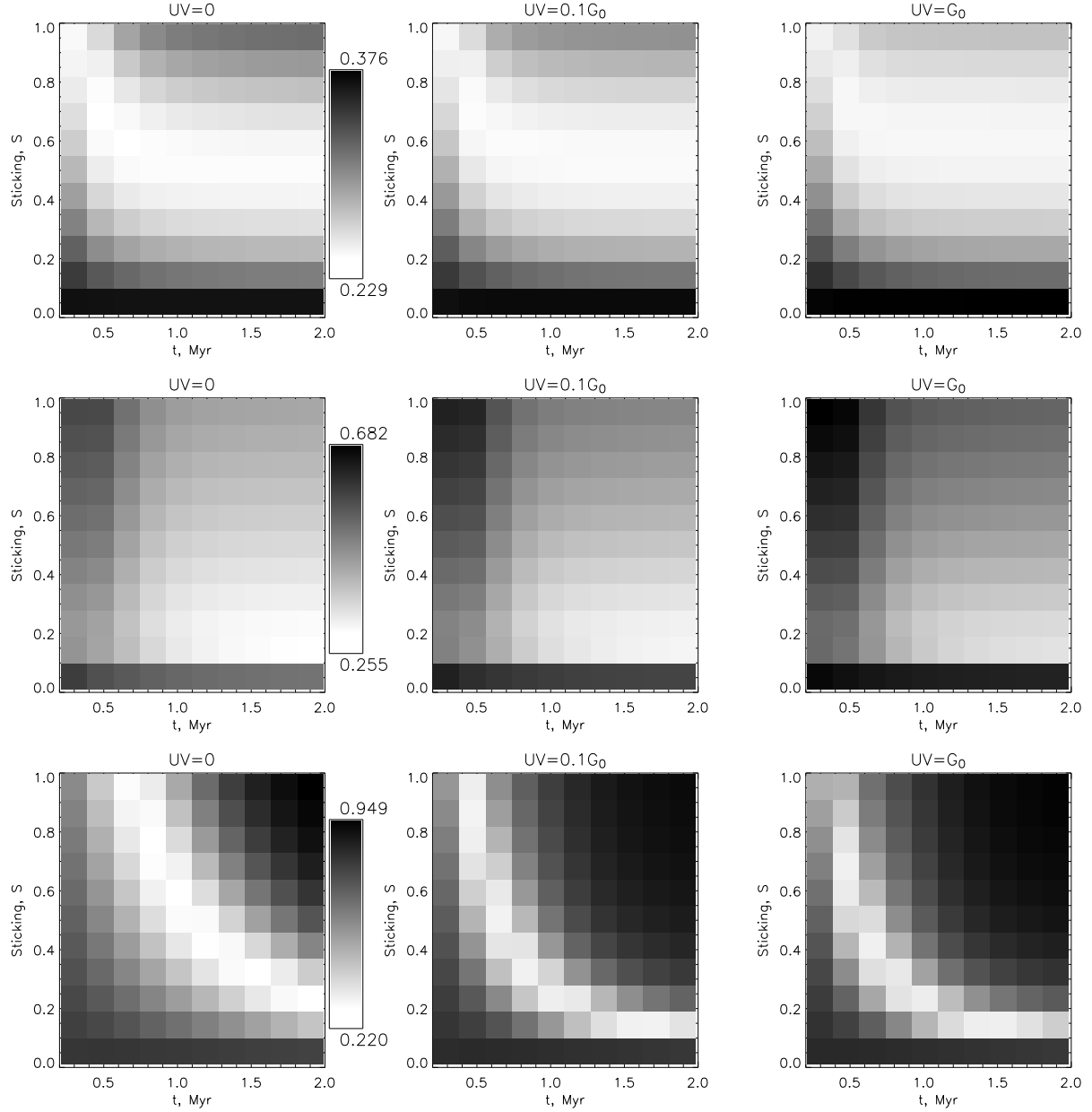


Fig. 6.— Values of SP-criterion (ts -diagrams) for optically thin transitions of C^{18}O (top row), H^{13}CO^+ (middle row), and C^{34}S (bottom row). Smaller values (lighter colors) correspond to better agreement. Columns differ by G values, indicated on top of each panel. The gradient scales on the right side of the first plot in each row are appropriate for all plots in the row.

All panels in Figure 6 indicate that values of S close to zero are ruled out. Higher sticking efficiencies are not favored in the analysis of the C^{18}O and H^{13}CO^+ transitions. However, it must be kept in mind that the range of SP is not very large for these transitions. This means that conclusions from their analysis must be taken with care.

The C^{34}S lines appear to be more robust discriminators between the model parameters. On the ts -diagram we clearly see the hyperbolic zone of best fitting with a significant range of $0.22 < \text{SP} < 0.95$. As might have been expected, smaller S values become appropriate as t_0 increases, as a lower sticking rate is compensated by a longer timescale.

In general, there are combinations of the studied parameters that provide a good agreement with observations, with SP values being less than 0.3 for all the optically thin transitions simultaneously. This corresponds to differences in the line intensities by a factor of 2. All the considered optically thin lines are not very sensitive to variations of the UV field. Indeed, they are mostly formed in the inner part of the core where the UV field is attenuated by the envelope.

3.3. Optically Thick Lines

Although the static model is quite successful in reproducing the observed optically thin line profiles, this should not be overinterpreted. Both the observed and modeled optically thin lines are nearly Gaussian in shape. The width of the theoretical profiles is defined by the adopted value of the microturbulent velocity. In our study this velocity is chosen to be 0.15 km s^{-1} in order to fit the observed line widths. Thus, for optically thin lines the quality of the fit in a static model depends mainly on the column density.

On the other hand, optically thick transitions are mostly sensitive to the conditions in the envelope, which makes them promising tracers of the external UV field. In our study, we consider the optically thick transitions of CS and HCO^+ . The ts -diagrams for these transitions are shown in Figure 7.

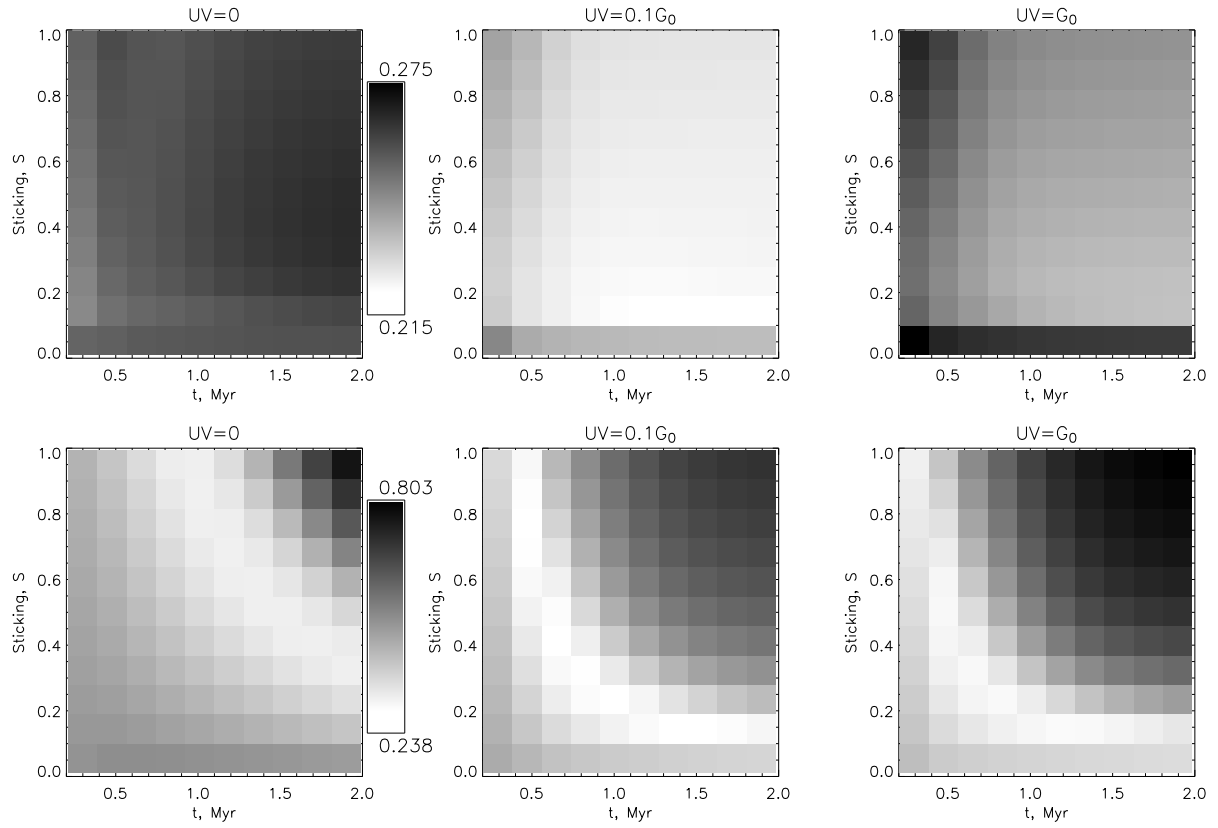


Fig. 7.— Values of SP for the optically thick transitions of HCO⁺ (top row) and CS (bottom row). Smaller values (lighter squares) correspond to better agreement. Columns differ by G values indicated on the top of each panel.

As expected, both the HCO^+ and CS diagrams are sensitive to variations of the UV radiation. In the case of no UV field (left panel), molecules survive in the envelope and produce emission over a broad range of impact parameters. In addition, enhancement of the molecules in the envelope leads to prominent dips in the profiles of optically thick lines. In contrast, a strong UV field, $G = 1$ (right panel), destroys molecules in the outer parts of the core, leading to more centrally peaked distributions of the integral intensity and to weaker self-absorption dips. Both effects worsen the agreement between observed and synthetic maps.

To demonstrate the influence of the UV field on the spectra, we show observed and theoretical spectral maps of CS(2-1) in Figure 8. For the static model with no UV radiation, $S = 0.6$ and $t = 0.8$ Myr CS line profiles have nearly the same intensity at all positions and self-absorption dips which are much deeper than in the observed spectra. The synthetic intensities of the model with strong UV field, $S = 0.6$, and $t = 0.4$ Myr decrease rapidly toward the edge of the core. The self-absorption dips become shallower than in the model without UV field.

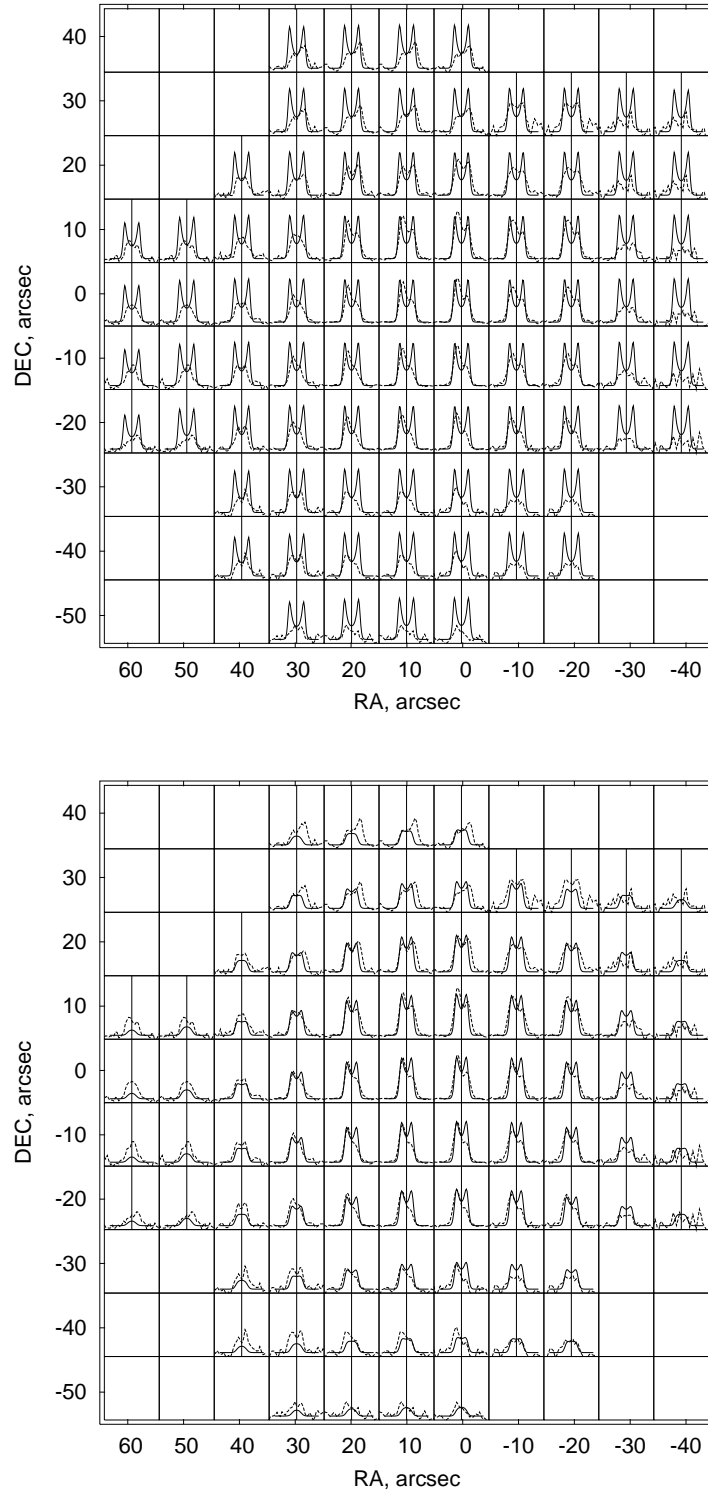


Fig. 8.— The map of the observed (blue) and modeled (red) CS(2-1) line profiles. In the top panel lines are calculated for the static model with $G = 0$, $S = 0.6$ $t = 0.8$ Myr. The bottom panel corresponds to the static model with $G = 1$, $S = 0.6$ $t = 0.4$ Myr.

According to Figure 7, the model with attenuated UV radiation ($G = 0.1$) seems to be most appropriate. It must be noted that it would be impossible to constrain the effect of the UV field using a central spectrum alone. One may argue that the excess intensity of the CS(2–1) line in the zero UV model can be mediated by an adjustment of the sulfur abundance which is not well constrained observationally. We computed two additional series of models with zero UV intensity and sulfur abundance decreased by a factor of 3 and 10, relative to our standard value. These models showed that a lower initial sulfur abundance leads to an overall decrease of S-bearing species in the core. These results in a better agreement for the central spectrum. However, the gradual decrease of the CS line intensity toward the outer boundary of the core can only be reproduced in models with some UV illumination.

Although the modeled optically thick lines have the expected double-peaked shape, these peaks are equal in height, contradicting the observed asymmetry. In order to describe this asymmetry, we must move from the static model toward a dynamical model. From Figures 6 and 7 it is obvious that the sticking efficiency is not well constrained in the static model. Therefore, the only parameter we will fix in dynamical models is the strength of the UV field ($G = 0.1$).

We will also not consider $t_0 < 0.4$ Myr values as they do not fit both the optically thin and optically thick lines. This seemingly minor limitation has an important implication for our dynamical models. The asymmetry of the central spectrum mentioned in the previous paragraph implies that the CB17 core undergoes an infall with a velocity of $\sim 0.05\text{--}0.1$ km s $^{-1}$. In the adopted prescription and for $t_0 > 0.4$ Myr such velocities are only possible with $\delta \geq 0.5$.

4. Results for the dynamical model

As described in § 2.1.2, the dynamical history of the core is represented by two parameters, which are the evolutionary time t_0 and the power law index δ . In the following, we investigate the sensitivity of molecular spectral maps to these parameters, at the same time searching for combinations of t_0 and δ which give the best agreement between observed and modeled CB17 maps.

Ideally, in order to find the ‘best-fit’ parameters for the CB17 core one should vary G , S , t_0 and δ , simultaneously. However, the primary goal of this paper is rather to show the general effect of the selected parameters. Therefore, we fix G to a value of 0.1 as determined from the static models, but vary S together with the dynamical parameters t_0 and δ .

In the dynamical modeling yet another parameter has to be considered. In the static

configuration we assumed the microturbulent velocity V_{turb} to be 0.15 km s^{-1} . This value is needed to reproduce the line width in the static model and as such it hardly leaves any room for a systematic velocity field. On the other hand, the central line asymmetry clearly shows that there is a non-zero infall velocity in the CB17 core. This seems to imply that V_{turb} is to be varied along with the other parameters. On the other hand, it obviously makes no sense to consider those values of V_{turb} which in combination with the systematic velocity would result in line widths that are too large or too small.

To minimize the needless effort, we adopted the following approach. For each combination of δ and t_0 we select V_{turb} to get the line width of about 0.15 km s^{-1} , so that the differences between theory and observations are only caused by disagreements in the line intensity and in the relative heights of blue and red peaks in optically thick lines.

4.1. Collapsing Core without Rotation

In purely collapsing models we only compare our results to the central spectrum of CB17 to avoid confusion with the effects of rotation. Results of the modeling are presented in Figure 9. We show SP values for three values of δ (0.5, 1.0, 1.5), vary t_0 between 0.4 and 4 Myr and S between 0 and 1. Only results for CS lines are given, as other molecules demonstrate much less sensitivity for the discussed parameters.

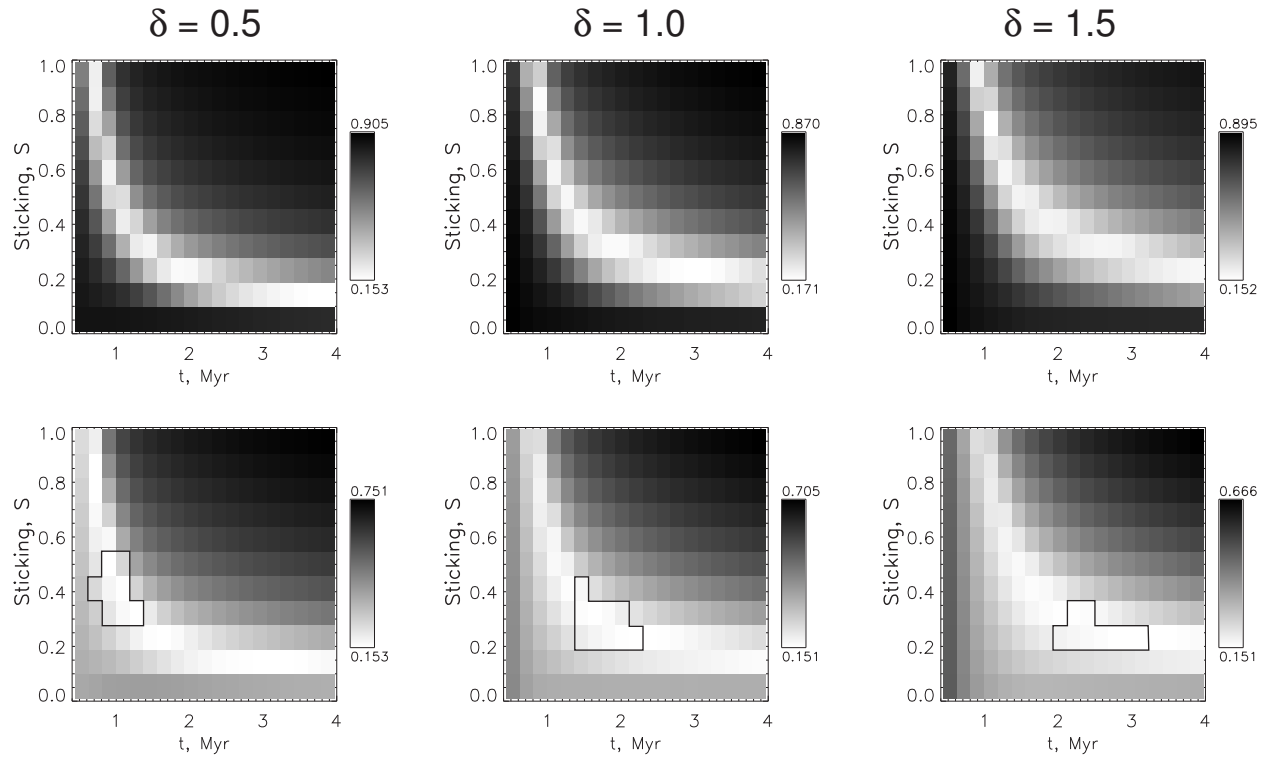


Fig. 9.— Values of SP for the optically thin C^{34}S transition (top row) and the optically thick CS transition (bottom row). Columns differ by δ values indicated on top of each panel. ‘Best-fit’ regions, selected by the blue-to-red peak intensity ratio, are shown by solid contours in the bottom row.

Figure 9 does not show any significant differences to the static model (see Figure 6, bottom panel, and Figure 7, bottom panel). In models with increasing δ the ‘best-fit’ region shifts toward later times which is expected, as larger δ values lengthen the ‘less-dense’ stage of core evolution. It seems that we have the same dilemma as in the static case, being unable to distinguish between large S and large t_0 . However, if we look at numeric SP values within the hyperbolic area, we see that the best-fit model for the CS transition (which is most sensitive to the infall velocity) corresponds to $S = 0.2 – 0.3$ for all three δ values.

The theoretical line profiles show that the agreement is still not perfect even in the ‘best-fit’ region. In some cases the line widths are different, in other cases the ratio between blue and red peaks is not the same as observed. The line width can be further adjusted with a more appropriate choice of V_{turb} . Thus, to split the contribution of the line width and the peak asymmetry in a ‘residual’ disagreement, we consider an additional criterion which is just the difference between the observed and the theoretical blue-to-red peak intensity ratios. Contours in the lower part of Figure 9 indicate models with the best agreement between theory and observations both in terms of the overall profile shape and the profile asymmetry. The combined selection procedure leads to the model parameters summarized in Table 3. Minimum SP values are selected only among locations within contours. The best-fit models are somewhat different for CS and C³⁴S.

Table 3: The ‘best-fit’ parameters for the dynamical model without rotation.

δ	t_0 , Myr	S	SP(CS)	SP(C^{34}S)
0.5	1.0–1.2	0.3–0.4	0.153	0.208
1.0	1.6–1.8	0.3	0.152	0.187
1.5	2.2–2.4	0.3	0.154	0.190

The data in Table 3 indicate that the sticking probability has an effective value of about 0.3, while the age of the core is larger than 1 Myr and probably less than 2.5 Myr. All presented SP values are smaller than in the corresponding static model. However, it must be kept in mind that these numbers are not directly comparable as they are computed for the central spectrum only in the case of the dynamical model, while in the static model SP values are calculated for the whole map.

The difference between SP values computed for various δ is small for C^{34}S and only marginal for CS. However, both transitions show a minor preference toward the model with $\delta = 1.0$. In the next subsection this model is used as an input for the 2D model. We emphasize that in the general case one may have to vary V_{turb} along with the other parameters.

4.2. Collapsing Core with Rotation

Finally, we now include rotation in the dynamical description of the core, the RT problem becoming two dimensional. In our model (§ 2.1.3), the rotation of the core is characterized by the initial angular velocity Ω . To simulate observations, we also have to specify the orientation of the core with respect to the observer, which is defined by the inclination angle i and the position angle PA. We assume that the core is observed edge-on ($i = 90^\circ$) in order to get an estimate of the minimum value of its angular momentum. No attempt is being made to reproduce the inclination angle as within the framework of a spherically symmetric model we are not able to distinguish between rapid rotation and low inclination. We tried several other values for i and found that variations of excitation conditions due to different rotation velocity profiles in the CB17 model are not strong enough to produce noticeable differences in observed spectra. It would be possible to determine i , using a more realistic dynamical model which would provide an independent information on the core rotation. Also, we note that it may be possible to estimate i independently for elongated cores from geometric reasoning.

The two parameters that are varied to get the best agreement with observations are the initial angular velocity Ω and the position angle PA. The position angle is defined as the angle between the projection of the core rotation axis on the sky and the direction to the North.

The simulation is made in the following way. The chemical structure of the core and its radial velocity field are taken from the best-fit 1D dynamical model with the parameters $\delta = 1.0$ and $t_0 = 1.6$ Myr. For the given Ω value we generate azimuthal velocities according to Eq. (4). These velocities are combined with the infall velocities to get the 2D velocity

field. This field is then used to solve the 2D radiation transfer equation. Having specified the PA, we calculate the convolved spectral map, which is further compared to the observed map using the SP criterion.

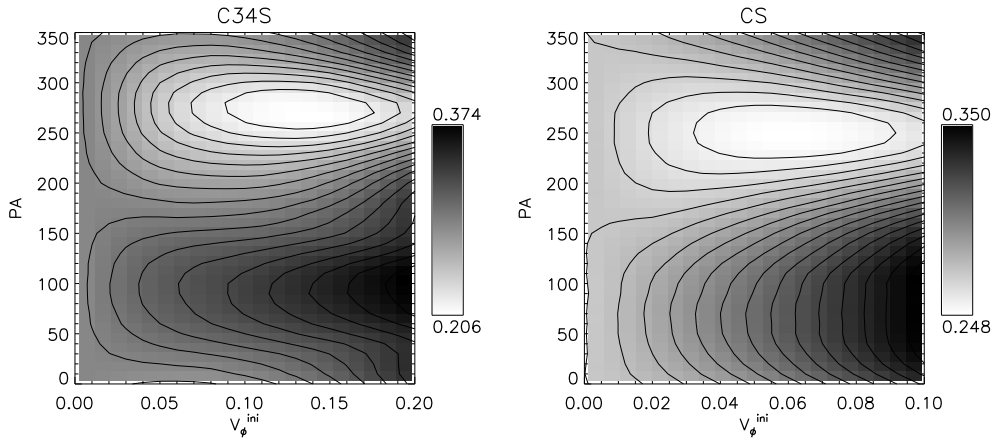


Fig. 10.— Values of SP for the optically thin C^{34}S transition (left) and for the optically thick CS transition (right) for various values of Ω and PA. Smaller values (lighter squares) correspond to better agreement. The x -axis is labeled in units of the initial linear rotation velocity at the edge of the core. A velocity of 0.1 km s^{-1} corresponds to $\Omega = 2.7 \times 10^{-14} \text{ s}^{-1}$.

Results of this comparison are shown in Figure 10. Obviously, when there is no rotation, the model shows no sensitivity to the PA value. As we increase Ω , both the optically thin and optically thick transitions show a clear preference to a PA value of $250^\circ - 300^\circ$. It is interesting to note that the sensitivity of the model to the position angle increases when we adopt Ω values that are greater than allowed observationally.

When the position angle is specified incorrectly, both transitions indicate that the model with pure infall agrees better with the observations than the model with infall and rotation (SP values increase from left to right in Figure 10). For $PA \approx 270^\circ$, SP values have minima at $V_\phi^{\text{ini}} = 0.13 \text{ km s}^{-1}$ for the C^{34}S line and at a somewhat smaller value of $V_\phi^{\text{ini}} = 0.07 \text{ km s}^{-1}$ for the CS line. The disagreement is probably caused by a higher rotation velocity closer to the core center (where the C^{34}S line is generated) than our model predicts. This can be further adjusted by adopting a different initial rotation velocity distribution. However, it must be noted that the optically thick CS line is in general less sensitive to Ω variations which is indicated by the smaller SP range. This implies that optically thin lines are better rotation indicators, at least, when the SP criterion or another similar width-sensitive criterion is used.

We note that the lowest SP values in the model with infall and rotation are actually higher than the corresponding values for the static model. This is caused by the values for V_{turb} adopted in the dynamical model. Because we did not try to vary V_{turb} along with the other parameters, the widths of some theoretical profiles do not quite fit those of their observed counterparts. This results in higher SP values.

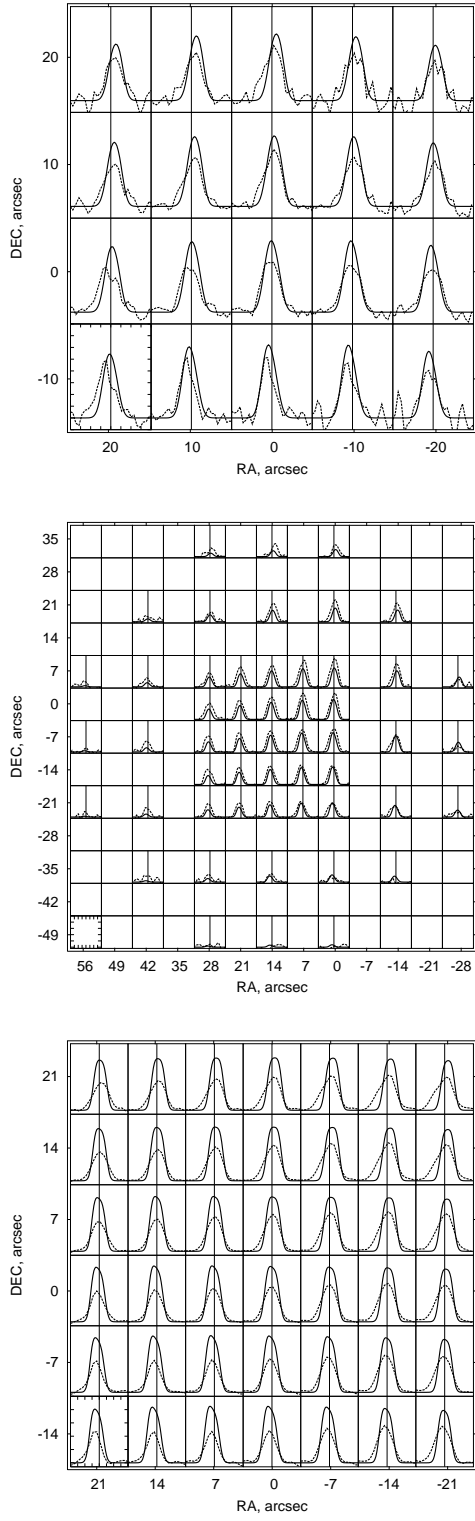


Fig. 11.— Spectral maps for the ‘best-fit’ CB17 model. Shown are optically thin transitions (from top to bottom— C^{34}S , H^{13}CO^+ , C^{18}O).

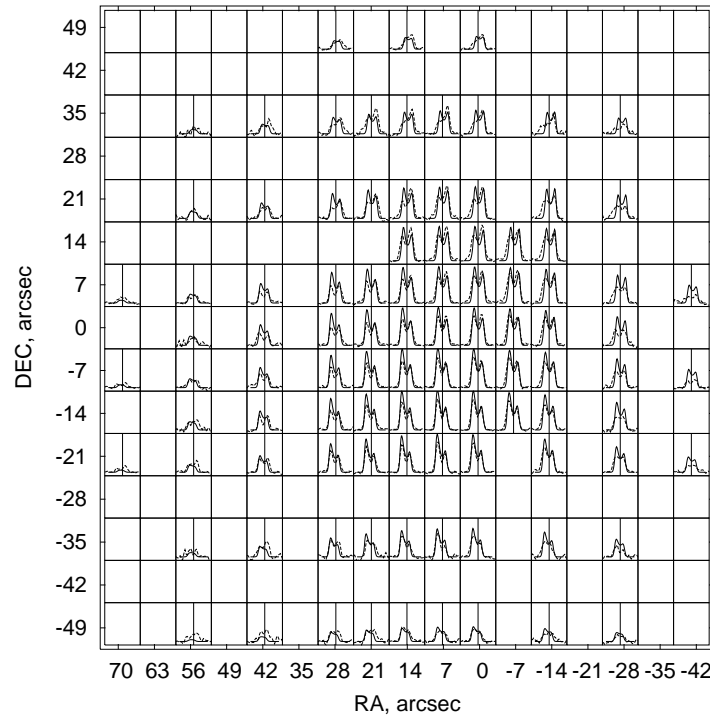
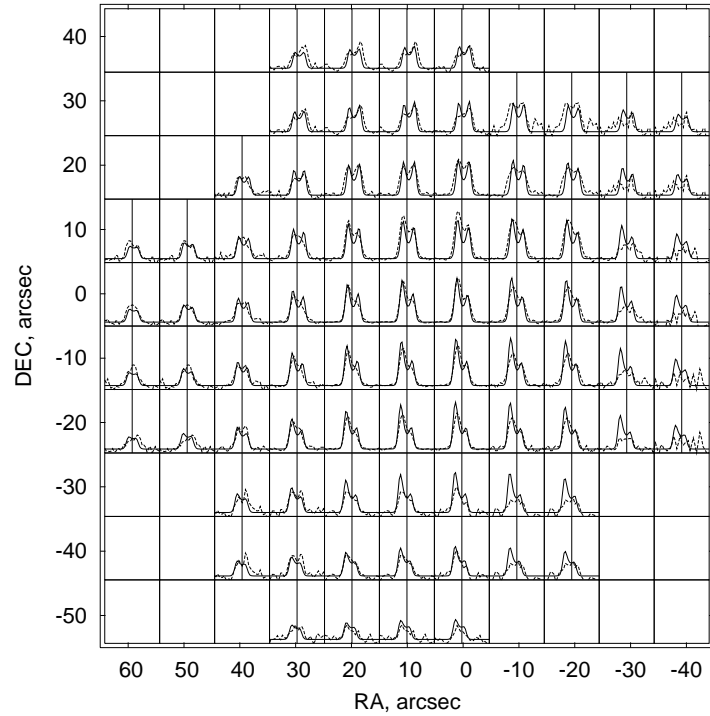


Fig. 12.— Same as in Figure 11 but for optically thick transitions (from top to bottom—CS, HCO^+).

Finally, in Figures 11 and 12 we show the convolved spectral maps of the CS(2-1), C³⁴S(2-1), HCO⁺(1-0), H¹³CO⁺(1-0), and C¹⁸O(2-1) lines for the ‘best-fit’ 2D model (Table 4). In all the modeled optically thin transitions shifts of the observed lines are reproduced quite successfully. Furthermore, the modeled optically thick CS profiles follow the asymmetry of the observed spectra, with blue-shifted profiles in the left bottom corner and nearly equal peak intensities in the upper part of the map. The consistency between the shapes of the theoretical and observed HCO⁺ profiles is less impressive. However, the theoretical line intensities are close to the observed ones, and the asymmetry is well reproduced in the central part of the map. The fit is worse in the upper part of the map, where there is some disagreement in the CS profiles as well. Given the overall consistency between maps of optically thin and optically thick lines, we believe this residual disagreement originates in the core structure which is certainly more complicated than the assumed spherical symmetry. It is also possible that there are some small-scale motions within the core that are not well described by the microturbulence model (like the motions discussed for B68 and L1489, see Introduction).

Table 4: The best-fit parameters for the dynamical model with rotation.

Parameter	Value
Chemical age	~ 2 Myr
The UV-field (G)	0.1
Effective sticking probability	0.3
δ	1.0
V_{rot}	0.1 km s $^{-1}$
V_{infall}	0.05 km s $^{-1}$
V_{turn}	0.1 km s $^{-1}$
PA	250°

In general, all the modeled maps do reproduce the spatial distributions of line intensities, except the C^{18}O (2-1) intensity, which is approximately 1.5–2 times greater than that observed. The C^{18}O overabundance is present in the static model as well and seems to follow from the adopted relatively low S value which is supposed to provide the best agreement for CS lines. Upper panels in Figure 6 indicate that regardless of UV intensity values $S > 0.5$ are preferred from the point of view of the C^{18}O abundance.

Some further adjustment of the CO abundance can be made with a variation in the cosmic ray ionization rate. However, there is a more natural explanation. In our study we assume that the $\text{C}^{16}\text{O}/\text{C}^{18}\text{O}$ ratio is constant and equal to 490 which is just the $\text{^{16}O}/\text{^{18}O}$ ratio. Due to the chemical fractionation the ratio $\text{C}^{16}\text{O}/\text{C}^{18}\text{O}$ can vary by a factor of a few (Federman et al. 2003). Specifically, the isotope-selective photodestruction of CO molecules may decrease the abundance of the isotopomer with the less abundant isotope (Bally & Langer 1982). Importantly, the fractionation apparently affects the $\text{C}^{16}\text{O}/\text{C}^{18}\text{O}$ ratio stronger than the $\text{^{12}CO}/\text{^{13}CO}$ ratio (Chu & Watson 1983; Federman et al. 2003), which would explain why we have the intensity disagreement in the C^{18}O lines, but not in the H^{13}CO^+ lines.

5. Discussion

This paper represents an attempt to develop a technique that allows to get as much information as possible from the spectral maps of a starless core. The technique is outlined in Figure 1. As an example, we used the CB17 core for which we have detailed observational data. This core appears to be quite young, having a chemical age of about 2 Myr. It is tempting to put it into an evolutionary sequence with other starless cores. Taking the central density as an indicator of the dynamical evolution, we have to assume that CB17 is quite evolved as it is almost as dense as L1544. From the point of view of the central depletion CB17 appears to be less evolved. There is some depletion in its center, which is indicated by high SP values for models with $S = 0$. In best-fit static models (e.g., $t_0 = 1$ Myr, $S = 0.4$) the CO molecule is depleted by a factor of 40 in the core center, and the CS molecule is depleted by a similar factor. However, this depletion is not very obvious in the CS column density distribution and is not seen at all in the CO column density distribution. This explains why the central holes are not seen in the observed maps of optically thin transitions of C^{34}S and C^{18}O . Within the classification scheme suggested by Lee et al. (2003) and Shirley et al. (2005), the CB17 core is *evolved dynamically and moderately evolved chemically*.

Within the framework of the adopted dynamical formalism we notice that ages greater than ~ 0.5 Myr and infall speeds of the order of 0.05 km s^{-1} are required. This implies $\delta > 0.5$ (the kinematic difference between the considered δ values of 0.5, 1.0, and 1.5 is

less significant). In this collapse regime the central density first stays almost constant and then undergoes a stage of a very fast growth. This conclusion is further illustrated by the comparison of the derived chemical age, $t_{\text{chem}} \approx 2$ Myrs, to the CB17 free-fall timescale, t_{ff} . For the assumed initial density of $n(\text{H}_2) = 5 \cdot 10^3 \text{ cm}^{-3}$, $t_{\text{ff}} = 0.4$ Myrs which is five times smaller than t_{chem} . So, formally we can conclude that the core has evolved more or less quasi-statically for $\sim 10^6$ years, then quickly lost stability and started to collapse. It seems reasonable just from mass conservation considerations that this is the appropriate scenario for a dense, collapsing, and chemically mature core. The scenario is similar to that favored by Shematovich et al. (2003) and considered by Lee et al. (2004). The quasi-static evolution of the starless core can result from the magnetic field support being gradually lost due to the ambipolar diffusion. On the other hand, Aikawa et al. (2005) and Keto & Field (2005) showed that quasi-static evolution of prestellar cores can be explained by the assumption that the initial condition for contraction represent a destabilized Bonnor-Ebert sphere.

The estimated CB17 age of 2 Myr may have implications for current theories of the star formation. For example, it is greater than the typical lifetime of dense cores found in gravoturbulent simulations (Vázquez-Semadeni et al. 2005) and the observationally estimated lifetimes of submillimeter cores studied by Kirk et al. (2005). So, one may ask how solid this estimate is. It must be noted from the static model that even if the core has spent the entire lifetime at constant central density of $n(\text{H}_2) = 5 \cdot 10^5 \text{ cm}^{-3}$, its chemical age is not less than 1 Myr. To make a more sounded estimate, which takes into account the density variations, we need to rely on our dynamical models. It is seen from Table 3 that, based on $\text{SP}(\text{C}^{34}\text{S})$ values, we can put “error bars” to the age estimate, so that it is 2 ± 0.4 Myr. But it must be kept in mind that this estimate is dependent on the adopted initial conditions. Therefore, it is of vital importance to constrain these conditions via models of the very early stages of prestellar core formation and evolution. Also, the dynamical history of CB17 can be refined with the same analysis applied to a more complicated dynamical model, which we plan to do in a forthcoming study.

Alternating asymmetry pattern in the CB17 core, i.e., changing blue-to-red asymmetry of optically thick lines and shifts of optically thin lines, indicate that the CB17 core rotates with an estimated azimuthal velocity of about 0.1 km s^{-1} . More precisely, the model core rotates differentially with a maximum rotation velocity of 0.13 km s^{-1} at 7000 AU from the core center. The corresponding angular momentum of the core can be estimated as

$$J = \frac{2}{5} M (R^{\text{U}})^2 \Omega \approx 2 \cdot 10^{56} \text{ g cm}^2 \text{ s}^{-1}. \quad (8)$$

Because of our assumption that the core is observed edge-on, this is the minimum angular momentum the core can have. Its value corresponds to the specific angular momentum of $1.6 \times 10^{21} \text{ cm}^2 \text{ s}^{-1}$, which is too high for a single star and somewhat higher than a

corresponding value for a star with a disk (e.g. Ohashi et al. 1997). On the other hand, it is close to specific angular momenta of binary T Tau stars (Simon et al. 1995). So, it seems that CB17 is going to fragment into at least two prestellar cores.

A possible drawback in using phenomenological descriptions is the possibility that the resulting model may be characterized by a combination of parameters that are mutually incompatible, like infall in a model where the thermal pressure exceeds the gravitational pressure. In order to check if our best-fit 2D model (Table 4) is physically consistent, we computed the gravitational force, the centrifugal force, and the pressure gradient as functions of radius. The analysis confirms our conclusion that the core is marginally gravitationally unstable as the gravitational force exceeds (in absolute value) the sum of forces, which counteract the collapse, by about 50%. In the inner part of the core the critical rotation velocity that would provide enough centrifugal support against collapse is only slightly higher than the velocity inferred from our study. This agrees with the very low infall velocity and demonstrates that in the inner parts of prestellar cores the rotation can be an important factor of core dynamics. The derived kinematic structure of the CB17 core corresponds to energy ratios $E_{\text{rot}}/E_{\text{grav}} \approx 0.03$, $E_{\text{therm}}/E_{\text{grav}} \approx 0.8$, and $E_{\text{turb}}/E_{\text{grav}} \approx 0.05$.

Our conclusions are affected to a certain degree by the choice of the probe molecules. All the lines we consider actually trace more the envelope of the core than its central region. Even optically thin lines of C^{18}O , H^{13}CO^+ , and C^{34}S are not good probes of the very center of the core because these species are depleted there. Deuterated and N-bearing species are more promising tracers of the inner core (e.g., van der Tak et al. 2005). Inspection of our chemical results shows that cyanopolyyne are especially sensitive not only to the age of an object, but also to the collapse regime. However, the analysis of cyanopolyne lines with the proposed technique is not straightforward, as it requires a more complicated approach to the radiation transfer modeling. Another possible limitation of our model is the neglect of UV heating. CB17 and other similar globules are often cometary shaped, suggestive of some outflow from the heated surface. Thus, UV irradiation affects not only the chemical, but also the thermal and the kinematic structure of the core. This is a promising topic for a more sophisticated dynamical model.

In this paper, we applied the ‘global’ SP criterion, which provides an estimate for the overall agreement between theoretical and observed spectra. However, as mentioned earlier, there are different features of real spectra that can be analyzed separately. For example, the depth of the self-absorption dip of optically thick lines is a good indicator of the UV field strength, while a good measure of the core rotation is given by relative shifts of optically thin lines. In the latter case the right thing to do is to compare the line center positions and not the overall profile shapes. The optically thin line intensities are sensitive to the

molecule column density, the blue-red asymmetry depends on the infall speed, and so forth. In this sense the global criterion is not the best choice as it has equally bad (large) values for a line which is wider than the observed one (easily adjusted with V_{turb} ; non-critical) as well as for a line which is shifted relative to the observed one (indicative of the wrong rotation model and/or the V_{LSR} velocity; critical). On the other hand, when applied with care, a SP-type criterion provides a useful global error control. The global criterion is a good starting point and must be refined in a later analysis. On the other hand, sometimes it can be complemented with more refined criteria that allow to study certain aspect of the model in detail or just to save the computational effort.

6. Conclusions

In this paper, we present a chemo-dynamical pilot study of the isolated Bok globule CB17 (L1389) based on the spectral maps of CS(2-1), C^{34}S (2-1), HCO^+ (1-0), H^{13}CO^+ (1-0), and C^{18}O (2-1) lines. A phenomenological model of a prestellar core evolution combined with time-dependent chemistry and a radiative transfer simulation of molecular lines is used to reconstruct the chemical and kinematical structure of this core as well as to study the influence of various physical factors on molecular line profiles. The main conclusions of the paper are:

1. We present a promising approach that allows to derive the chemical and kinematic structure of a prestellar core from its spectral maps. We analyze both optically thick and optically thin lines, center and off-center positions, various species and transitions etc. We show that even when this detailed information is available, it is not trivial to construct a consistent core model.
2. Among the considered molecules, CS and its isotopomer C^{34}S turned out to be most sensitive species to variations in model parameters and can be used to reconstruct the dynamical history of prestellar cores. As the effects of the age and sticking probability (S) are quite similar for this molecule, it is desirable to have more qualitative information on the S value.
3. UV irradiation is an important factor affecting the chemistry and, correspondingly, line profiles in prestellar cores even when the strength of UV field is much smaller than the average interstellar value. The attenuated UV field ($G = 0.1$) is needed to explain distributions of intensities and self-absorption features of the observed CB17 spectral maps. Optically thick lines tracing the envelope are mostly sensitive to the UV field.

4. The chemical age of the core is about 2 Myr. All the considered species (CO, HCO^+ , and CS) are depleted in the inner core, but the degree of depletion is still not high enough to show up in the integrated intensity maps. This allows to classify this core as evolved dynamically and moderately evolved chemically. The best-fit sticking probability value for the core is $S = 0.3 - 0.5$. This is an effective value that may be higher if we miss some important desorption mechanism.
5. The changing asymmetry pattern of the optically thick line profiles over the cloud surface as well as shifts of the optically thin lines are both indicative of a complex kinematical structure of the core. We argue that the observed maps are reasonably well reproduced by a model with slow infall (0.05 km s^{-1}), differential rotation (0.1 km s^{-1}), and microturbulence (0.1 km s^{-1}). From the derived angular momentum, we conclude that CB17 is likely to fragment and to form a binary (multiple) star.
6. While being artificial in nature, our phenomenological approach allows to reveal crucial parameters that must be considered in attempts to compare observations with results of more sophisticated physical models based on combined MHD, chemical and radiative transfer simulations.

We are grateful to B. Shustov, A. Tutukov (INASAN), and D. Semenov (MPIA) for fruitful discussions and to the referee for helpful comments. This study is supported by the DFG grant “Molecular Cloud Chemistry” HE 1935/21-1. YP and DW also acknowledge support from the RFRB grant 04-02-16637. DW acknowledges support from the RF President Grant NSh-162.2003.2.

REFERENCES

Aikawa, Y., Herbst, E., Roberts, H., Caselli, P. 2005, ApJ, 620, 330

Bally, J., Langer, W. D. 1982, ApJ, 255, 143

Belloche, A., André, P., Despois, D., Blinder, S. 2002, A&A, 393, 927

Benson, P. J., Caselli, P., Myers, P. C. 1998, ApJ, 506, 743

Caselli, P., Benson, P. J., Myers, P. C., Tafalla, M. 2002, ApJ, 572, 238

Chu, Y.-H., Watson, W. D. 1983, ApJ, 267, 151

Draine, B. T. 1978, *ApJS*, 36, 595

Evans, N. J. II. 1999, *ARA&A*, 37, 311

Federman, S. R., Lambert, D. L., Sheffer, Y., Cardelli, J. A., Andersson, B.-G., van Dishoeck, E. F., Zsargó, J. 2003, *ApJ*, 591, 986

Flower, D. R., Pineau des Forets, G., Walmsley, C. M. 2005, *A&A*, 436, 933

Geppert, W. D., Thomas, R., Semaniak, J., Ehlerding, A., Millar, T. J. et al. 2004, *ApJ*, 609, 459

Gregeresen, E. M., Evans, N. J., II. 2000, *ApJ*, 538, 260

Hasegawa, T. I., Herbst, E. 1993, *MNRAS*, 263, 589

Hogerheijde, M. R., van der Tak, F. F. S. 2000, *A&A*, 362, 697

Jijina, J., Myers, P. C., Adams, F. C., 1999, *ApJS*, 125, 161

Kirk, J. M., Ward-Thompson, D., & André, P. 2005, *MNRAS*, 360, 1506

Kane, B. D., Clemens, D. P. 1997, *AJ*, 113, 1799

Keto, E., Field, G. 2005, *ApJ*, 635, 1151

Lada, Ch. J., Bergin, E. A., Alves, J. F., Huard, T. L. 2003, *ApJ*, 586, 286

Lee, H.-H., Herbst, E., Pineau des Forets, G., Roueff, E., Le Bourlot, J. 1996, *A&A*, 311, 690

Lee, Ch. W., Myers, P. C., Tafalla, M. 2001, *ApJS*, 136, 703

Lee, J.-E., Evans, N. J., II, Shirley, Y. L., Tatematsu, K. 2003, *ApJ*, 583, 789

Lee, J.-E., Bergin, E. A., Evans, N. J., II. 2004, *ApJ*, 617, 360

Lee, J.-E., Evans, N. J., II, Bergin, E. A. 2005, *ApJ*, 631, 351

Lemme, C., Wilson, T. L., Tieftrunk, A. R., Henkel, C. 1996, *A&A*, 312, 585

Millar, T. J., Farquhar, P. R. A., Willacy, K. 1997, *A&AS*, 121, 139

Myers, P. 2005, *ApJ*, 623, 280

Ohashi, N., Hayashi, M., Ho, P. T. P., Momose, M., Tamura, M., Hirano, N., Sargent, A. I. 1997, *ApJ*, 488, 317

Pavlyuchenkov, Ya. N., Shustov, B. M. 2004, *Astronomy Reports*, 48, 315

Rawlings, J. M. C., Yates, J. A. 2001, *MNRAS*, 326, 1423

Redman, M. P., Keto, E., Rawlings, J. M. C., Williams, D. A. 2004, *MNRAS*, 352, 1365

Schöier, F. L., van der Tak, F. F. S., van Dishoeck, E. F., Black, J. H. 2005, *A&A*, 432, 369

Semenov, D., Wiebe, D., Henning, Th. 2004, *A&A*, 417, 93

Shematovich, V. I., Wiebe, D. S., Shustov, B. M., Li, Zhi-Yun, 2003, *ApJ*, 588, 894

Shirley, Y. L., Nordhaus, M. K., Grcevich, J., M., Evans, N. J., II, Rawlings, J. M. C., Tatematsu, K. 2005, *ApJ*, 632, 982

Simon, M., Ghez, A. M., Leinert, Ch., Cassar, L., et al. 1995, *ApJ*, 443, 625

Tafalla, M., Mardones, D., Myers, P. C., Caselli, P., Bachiller, R., Benson, P. J. 1998, *ApJ*, 504, 900

Tafalla, M., Myers, P. C., Caselli, P., Walmsley, C. M., Comito, C. 2002, *ApJ*, 569, 815

Tafalla, M., Myers, P. C., Caselli, P., Walmsley, C. M. 2004, *A&A*, 416, 191

Turner, B. E. 1995, *ApJ*, 449, 635

Turner, B. E. 1996, *ApJ*, 468, 694

Turner, B. E., Pirogov, L., Mihm, Y.C. 1997, *ApJ*, 483, 235

Turner, B. E., Lee, H.-H., Herbst, E. 1998, *ApJS*, 115, 91

Vázquez-Semadeni, E., Kim, J., Shadmehri, M., & Ballesteros-Paredes, J. 2005, *ApJ*, 618, 344

van der Tak, F. F. S., Caselli, P., Ceccarelli, C. 2005, *A&A*, 439, 195

Whitworth, A. P., Ward-Thompson, D. 2001, *ApJ*, 547, 317

Wiebe, D., Semenov, D., Henning, Th. 2003, *A&A*, 399, 197

Williams, J. P., Myers, P. C., Wilner, D. J., di Francesco, J. *ApJ*, 513, L61